

Journal of Biomedical Optics

BiomedicalOptics.SPIEDigitalLibrary.org

Light-activatable cannabinoid prodrug for combined and target- specific photodynamic and cannabinoid therapy

Xiaoxi Ling
Shaojuan Zhang
Yang Liu
Mingfeng Bai

SPIE.

Xiaoxi Ling, Shaojuan Zhang, Yang Liu, Mingfeng Bai, "Light-activatable cannabinoid prodrug for combined and target-specific photodynamic and cannabinoid therapy," *J. Biomed. Opt.* **23**(10), 108001 (2018), doi: 10.1117/1.JBO.23.10.108001.

Light-activatable cannabinoid prodrug for combined and target-specific photodynamic and cannabinoid therapy

Xiaoxi Ling,^a Shaojuan Zhang,^a Yang Liu,^b and Mingfeng Bai^{a,c,d,e,*}

^aUniversity of Pittsburgh, Department of Radiology, Pittsburgh, Pennsylvania, United States

^bVanderbilt University Institute of Imaging Sciences, Nashville, Tennessee, United States

^cUniversity of Pittsburgh, Department of Medicine, Pittsburgh Pennsylvania, United States

^dUniversity of Pittsburgh, Department of Bioengineering, Pittsburgh, Pennsylvania, United States

^eUniversity of Pittsburgh Cancer Institute, Pittsburgh, Pennsylvania, United States

Abstract. Cannabinoids are emerging as promising antitumor drugs. However, complete tumor eradication solely by cannabinoid therapy remains challenging. In this study, we developed a far-red light activatable cannabinoid prodrug, which allows for tumor-specific and combinatory cannabinoid and photodynamic therapy. This prodrug consists of a phthalocyanine photosensitizer (PS), reactive oxygen species (ROS)-sensitive linker, and cannabinoid. It targets the type-2 cannabinoid receptor (CB₂R) overexpressed in various types of cancers. Upon the 690-nm light irradiation, the PS produces cytotoxic ROS, which simultaneously cleaves the ROS-sensitive linker and subsequently releases the cannabinoid drug. We found that this unique multifunctional prodrug design offered dramatically improved therapeutic efficacy, and therefore provided a new strategy for targeted, controlled, and effective antitumor cannabinoid therapy. © 2018 Society of Photo-Optical Instrumentation Engineers (SPIE) [DOI: 10.1117/1.JBO.23.10.108001]

Keywords: light-activatable prodrug; photodynamic therapy; cannabinoid; CB₂R; combination therapy.

Paper 180273R received May 14, 2018; accepted for publication Sep. 19, 2018; published online Oct. 17, 2018.

1 Introduction

Photodynamic therapy (PDT) is an attractive treatment strategy that is minimally invasive with little to no systemic toxicity.^{1,2} PDT utilizes photosensitizers (PSs) to harvest the power of light and transform it into reactive oxygen species (ROS), a powerful cancer-killing grenade. The ROS are short-lived, limiting the effect of PDT to the irradiated area only. Currently, several drugs have been approved across the globe for PDT treatment. Most notably, Photofrin[®] was approved back in 1993 in Canada for bladder cancer treatment and later for other cancers and diseases by FDA in the US and other regions in the world.³ A major drawback of common PSs is their lack of specific uptake. Even though PDT toxicity is limited in the region exposed to light irradiation only, normal cells in the same region still suffer from unnecessary PDT damage. This limitation can be overcome by adding targeting ligand to the PS design. With the introduction of a targeting moiety, PDT benefits from two advantages: (1) specific targeting can lead to significant higher uptake in malignant cells, which leads to more efficient treatment outcome with fewer damage to innocent cells and (2) lower dose of PSs would be needed for similar therapeutic efficacy, which further lowers side effects of the treatment. Previously, our lab developed PDT agents that specifically target type-2 cannabinoid receptor (CB₂R)^{4,5} or translocator protein^{6,7} with successful anticancer therapy outcome in murine tumor models.

In addition to targeting functionality, a new advance of PDT agent design is to include ROS-cleavable linker for on-demand drug release. We developed a heterobifunctional thioketal linker

for such a purpose.⁸ The You laboratory recently reported several prodrugs that can be activated by ROS produced from PS and encouraging combinatory therapeutic effects have been observed.⁹⁻¹² For example, they synthesized a light-activatable paclitaxel prodrug for combined PDT and chemotherapy.¹³ As compared to the non-ROS-cleavable analog, this light-activatable paclitaxel prodrug showed greatly improved therapeutic outcome in ovarian cancer cells. However, this prodrug has aggregation issues in aqueous solution and its lack of targeting functionality. In a more recent study, polyethylene glycolylated folic acid molecules with different sizes of polyethylene glycol (PEG) were attached to the light-activatable paclitaxel prodrug for improved water solubility and targeted delivery.¹⁴ Unfortunately, these targeted prodrugs still suffer from aggregation issue and the structures involve many components, including a phthalocyanine PS, folic acid, PEG, ROS-cleavable linker and paclitaxel. It is more desirable to develop a water soluble, targeted, and light activatable prodrug with a relatively simple design.

In this study, we synthesized a light-activatable cannabinoid prodrug, IR700DX-TK-*mbc*94, for combined and target-specific PDT and cannabinoid therapy. This prodrug consists of only three components: a highly hydrophilic phthalocyanine PS, ROS-sensitive thioketal linker, and cannabinoid. Cannabinoids have attracted great attention as promising antitumor drugs as they can produce ROS, inhibit pro-metastatic Id1 gene expression, and upregulate autophagy-mediated cell death.¹⁵ The cannabinoid molecule we chose targets CB₂R overexpressed in various types of cancers, such as glioma, lymphoma, skin, prostate, lung, and breast cancer.^{16,17} Upon light irradiation,

*Address all correspondence to: Mingfeng Bai, E-mail: mingfeng.bai@vanderbilt.edu

the PS produces cytotoxic ROS, which simultaneously cleaves the ROS-sensitive linker and subsequently releases cannabinoid drug. Therefore, this prodrug offers targeted and on-demand combinatory PDT and cannabinoid therapy with a simple design. We found that treatment with IR700DX-TK-*mbc94* caused remarkably improved therapeutic outcome as compared to nonactivatable IR700DX-*mbc94*.

2 Materials and Methods

2.1 General

All solvents used are of ACS or HPLC grade (Fisher Scientific, Pittsburgh, Pennsylvania). The PS, IR700DX-NHS ester, was purchased from LI-COR Bioscience (Lincoln, Nebraska). ^1H and ^{13}C NMR spectra were recorded at 25°C on the Bruker Avance III 400 MHz. Unless otherwise specified, chemical shifts δ were expressed in parts per million (ppm) based on tetramethylsilane (TMS) in CDCl_3 (δ 0.00 ppm), residue dimethyl sulfoxide (DMSO) (δ 2.50 ppm), or residue CHCl_3 (δ 77.16 ppm), and coupling constants J are given in Hz. Coupling patterns are abbreviated as s (singlet), d (doublet), t (triplet), q (quartet), quin (quintet), dd (doublet of doublets), ddd (doublet of doublet of doublets) and m (multiplet). Electrospray mass spectra were recorded on SYNAPT G2S TOF-MS mass spectrometer (Waters, Milford, Massachusetts) in positive ion mode. 7-Diethylamino-3-(4'-maleimidylphenyl)-4-methylcoumarin (CPM) was obtained from Fischer Scientific. The following instruments, supplies and assay kits were used for *in vitro* studies: Synergy™ H4 Hybrid Multi-Mode Microplate Reader (BioTek, Winooski, VT), 96-well optical black plates (Fisher Scientific), CellTiter-Glo Luminescent Cell Viability Assay kit (Promega, Madison, Wisconsin).

2.2 Synthesis of IR700DX-TK-*mbc94*

Mbc94,¹⁸ IR700DX-*mbc94*,⁶ and heterobifunctional thioetheral linker **1**⁸ were synthesized based on previously reported methods.

5-(4-chloro-3-methylphenyl)-1-(4-(20,20,20-trifluoro-14,14-dimethyl-10,19-dioxo-13,15-dithia-2,9,18-triazacosyl)benzyl)-N-((1R,4R)-1,3,3-trimethylbicyclo[2.2.1]heptan-2-yl)-1H-pyrazole-3-carboxamide (**2a**): The heterobifunctional thioetheral linker **1** (7.0 mg, 22 μmol) and N,N,N',N'-Tetramethyl-O-(1H-benzotriazol-1-yl)uronium hexafluorophosphate (HBTU) (9.5 mg, 25 μmol) were dissolved in dimethylformamide (DMF) (1.25 mL) at 0°C. Diisopropylethylamine (DIEA) (6.3 μL , 67 μmol) was added to the mixture. The mixture was stirred in ice bath for 2 h. Next, a solution of *mbc94* (14 mg, 20 μmol) in DMF (0.20 mL) was added to the mixture. The resulting mixture was then warmed to room temperature and stirred for additional 2 h. The reaction mixture was quenched by water (0.5 mL) and evaporated to dryness. The resulting mixture was separated using column chromatography with an eluent of dichloromethane/methanol = 100:6 to yield **2a** (14 mg, 80%) as a clear oil. ^1H NMR (400 MHz, chloroform-*d*, TMS) δ 8.06 (br s, 1H), 7.40 (d, J = 8.0 Hz, 2H), 7.33 (d, J = 8.2 Hz, 1H), 7.13 (d, J = 1.8 Hz, 1H), 7.07–6.97 (m, 3H), 6.91 (d, J = 9.8 Hz, 1H), 6.74 (s, 1H), 6.44 (br m, 1H), 5.32 (s, 2H), 4.12 (s, 2H), 3.74 (d, J = 9.6 Hz, 1H), 3.68 (quin., J = 6.7 Hz, 1H), 3.53 (q, J = 6.0 Hz, 2H), 3.16 (q, J = 7.4 Hz, 1H), 3.11 (q, J = 6.3 Hz, 2H), 3.01–2.90 (m, 2H), 2.81 (t, J = 7.0 Hz, 4H), 2.78 (s, 1H), 2.45 (t, J = 6.8 Hz, 2H), 2.32 (s, 3H), 1.80 (d, J = 2.4 Hz, 1H),

1.76–1.58 (m, 4H), 1.54 (s, 7H), 1.47–1.35 (m, 9H), 1.35–1.16 (m, 9H), 1.12 (s, 3H), 1.08 (s, 3H), 0.84 (s, 3H). ^{13}C NMR (100 MHz, chloroform-*d*, TMS) 172.1, 162.8, 157.7 (q, J = 36.5 Hz), 146.1, 145.2, 144.7, 138.0, 137.9, 137.5, 136.9, 135.6, 134.7, 131.5, 131.4, 131.2, 130.3, 129.6, 129.2, 128.4, 127.8, 127.41, 127.40, 127.1, 116.0 (q, J = 286 Hz), 106.7, 77.3, 63.4, 56.4, 55.3, 53.4, 51.9, 48.6, 48.1, 48.0, 43.3, 42.7, 40.8, 39.6, 39.2, 39.1, 38.6, 35.5, 31.0, 30.8, 29.7, 29.0, 28.8, 27.3, 26.1, 26.0, 25.8, 25.6, 25.5, 21.3, 20.0, 19.9, 19.7, 17.8. MS electrospray ionization (ESI): m/z = 891.4052, calcd. for $\text{C}_{45}\text{H}_{63}\text{ClF}_3\text{N}_6\text{O}_3\text{S}_2^+$ m/z (M + H)⁺ = 891.4038.

1-(4-(17-amino-14,14-dimethyl-10-oxo-13,15-dithia-2,9-diazaheptadecyl)benzyl)-5-(4-chloro-3-methylphenyl)-N-((1R,4R)-1,3,3-trimethylbicyclo[2.2.1]heptan-2-yl)-1H-pyrazole-3-carboxamide (**2b**): A solution of 2.4 M lithium hydroxide in water (50 μL , 0.12 mmol) was added to a solution of trifluoroacetamide **2a** (14 mg, 16 μmol) methanol (1.0 mL). The reaction mixture was heated at 50°C for 4 h. The reaction mixture was evaporated to dryness and the product was purified using column chromatography with an eluent of dichloromethane/methanol/ammonia = 100:10:0.1 to 100:20:0.1 to 100:100:0.1 to yield **2b** (9.8 mg, 79%). ^1H NMR (400 MHz, chloroform-*d*, TMS) δ 9.71 (br s, 2H), 8.15 (br s, 3H), 7.42 (d, J = 8.2 Hz, 2H), 7.36 (d, J = 8.2 Hz, 1H), 7.15 (dd, J = 1.9, 0.4 Hz, 1H), 7.09 (s, 1H), 7.07 (s, 1H), 7.02 (ddd, J = 8.2, 2.2, 0.6 Hz, 1H), 6.90 (d, J = 9.6 Hz, 1H), 6.79 (s, 1H), 5.96 (t, J = 6.0 Hz, 1H), 5.30 (s, 2H), 4.09 (br s, 2H), 3.80 (dd, J = 9.7, 1.5 Hz, 1H), 3.20 (quin., J = 6.7 Hz, 2H), 3.11 (br s, 2H), 2.98–2.87 (m, 5H), 2.44 (t, J = 6.2 Hz, 2H), 2.35 (s, 3H), 1.80 (d, J = 3.3 Hz, 1H), 1.77–1.63 (m, 4H), 1.58 (s, 6H), 1.53–1.44 (m, 3H), 1.44–1.36 (m, 3H), 1.36–1.21 (m, 6H), 1.16 (s, 3H), 1.11 (s, 3H), 0.87 (s, 3H).

IR700DX-TK-*mbc94* (**3**): IR700DX-NHS (4 mg, 2 μmol) and **2b** (9.8 mg, 12 μmol) were dissolved in DMSO (1 mL). The resulting mixture was stirred under Ar atmosphere and dark condition at room temperature for 2 days. Water (15 mL) was added before the mixture was lyophilized to give a green paste. The solid residue was washed with ethyl acetate (5.0 mL \times 3) and redissolved in methanol. The methanol solution was evaporated to dryness and dried under vacuum to yield compound **3** as a green powder (2.2 mg, 41%). ^1H NMR (400 MHz, DMSO-*d*6) δ 9.68 (m, 5H), 9.54 (m, 1H), 9.35 (d, J = 7.5 Hz, 1H), 8.48–8.34 (m, 7H), 7.98 (d, J = 8.2 Hz, 1H), 7.37 (d, J = 8.3 Hz, 2H), 7.31 (d, J = 8.2 Hz, 1H), 7.29–7.22 (m, 2H), 7.11 (dd, J = 8.1, 2.1 Hz, 1H), 7.00 (d, J = 8.0 Hz, 2H), 6.78 (s, 1H), 5.42 (s, 2H), 4.94 (t, J = 5.6 Hz, 2H), 4.05 (s, 2H), 3.69 (s, 1H), 3.13–3.02 (m, 5H), 2.91–2.81 (m, 4H), 2.81–2.62 (m, 30 H), 2.37 (t, J = 7.3 Hz, 2H), 2.26 (s, 3H), 2.12 (t, J = 7.6 Hz, 2H), 2.00–1.90 (m, 4H), 1.84 (s, 1H), 1.75–1.70 (m, 1H), 1.70–1.50 (m, 20H), 1.47 (s, 6H), 1.45–1.37 (m, 5H), 1.36–1.11 (m, 7H), 1.08 (s, 3H), 1.00 (s, 3H), 0.78 (s, 3H), –1.03 (s, 4H), –2.19 (s, 4H), –2.85 (s, 12H). MS (ESI): m/z = 1355.6840, calcd. for $\text{C}_{114}\text{H}_{158}\text{ClN}_{17}\text{Na}_6\text{O}_{27}\text{S}_8\text{Si}_3^{2+}$ m/z (M + 6Na)²⁺ = 1355.3842 (Fig. 1).

2.3 Synthesis of *mbc94-SH* and *mbc94-TTPA*

3-(Tritylthio)propionic acid 5.9 mg (17 μmol), HBTU (8 mg, 21 μmol), and DIEA (3.9 mg, 30 μmol) were dissolved in anhydrous DMF (0.6 mL) under argon atmosphere at 0°C with stirring. *Mbc94* (12 mg, 17 μmol) dissolved in anhydrous DMF (0.6 mL) was added dropwise to the mixture after which the

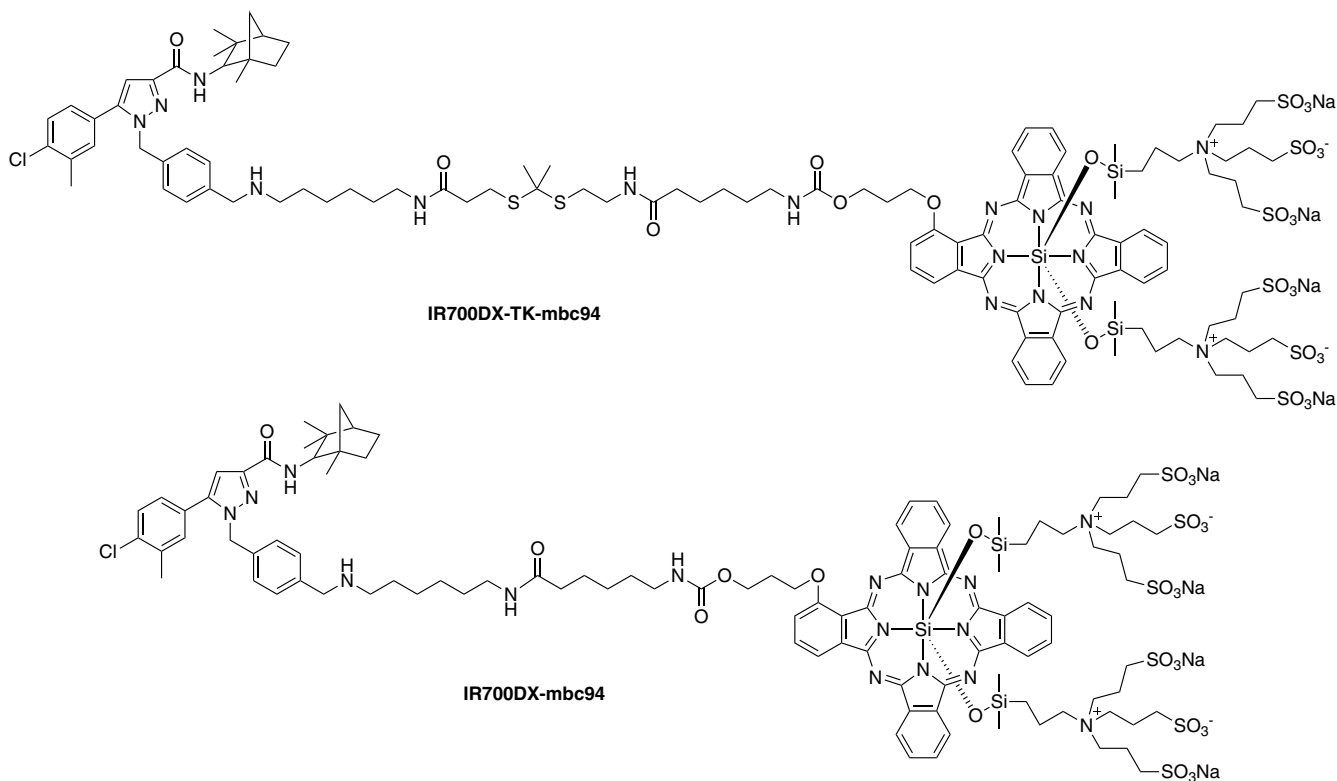


Fig. 1 Structures of IR700DX-TK-*mbc94* and IR700DX-*mbc94*.

reaction mixture was slowly warmed to room temperature and stirred for additional 16 h. The resulting mixture was dried and separated by column chromatography using a gradient of 2% to 5% methanol in dichloromethane. The desired product (*mbc94*-TTPA) was yielded as an oil (10.7 mg). The trityl protection was subsequently removed by dissolving the product in dichloromethane (1.0 mL) and trifluoroacetic acid (0.3 mL) at -20°C followed by addition of triethylsilane (50 μL). After removal of solvent, the mixture was separated by column chromatography using a mixture of dichloromethane/methanol/ammonia = 100:5:0.5 to yield the final compound (*mbc94*-SH) as an oil (1 mg, 7% after two steps).

^1H NMR of ***mbc94*-TTPA** (400 MHz, CDCl_3) δ 7.44-7.36 (m, 7 H), 7.36-7.30 (m, 2H), 7.29-7.17 (m, 7H), 7.17-7.10 (m, 2H), 7.07-6.91 (m, 4H), 6.81 (s, 1H), 5.62 (t, $J = 8.1$ Hz, 1H), 5.29 (s, 2H), 3.94 (s, 1H), 3.80 (dd, $J = 12.7, 1.7$ Hz, 1H), 3.08 (q, $J = 9.1$ Hz, 2H), 3.00-2.86 (m, 4H), 2.76 (t, $J = 9.5$ Hz, 2H), 2.50-2.42 (m, 2H), 3.28 (s, 1H), 2.22 (t, $J = 9.4$ Hz, 1H), 2.05 (t, $J = 9.4$ Hz, 1H), 1.82-1.18 (m, 17H), 1.16 (s, 3H), 1.10 (s, 3H), 0.85 (s, 3H).

^1H NMR of ***mbc94*-SH** (400 MHz, CDCl_3) δ 7.33 (t, $J = 10.0$ Hz, 3H), 7.19-6.87 (m, 6H), 6.79 (s, 1H), 5.62 (t, $J = 8.1$ Hz, 1H), 6.66-6.45 (br s, 1H), 5.25 (s, 2H), 3.88 (s, 2H), 3.80 (dd, $J = 13.1, 1.9$ Hz, 1H), 3.20 (q, $J = 9.2$ Hz, 2H), 3.00 (t, $J = 8.9$ Hz, 2H), 2.75 (t, $J = 9.4$ Hz, 2H), 2.56 (t, $J = 8.7$ Hz, 2H), 2.33 (s, 1H), 1.84-1.92 (m, 17H), 1.25 (s, 3H), 1.17 (s, 3H), 1.10 (s, 3H).

2.4 Competitive Binding Study

The binding affinities of IR700DX-TK-*mbc94*, IR700DX-*mbc94*, and *mbc94*-SH to human CB_2 receptor were determined using established radioligand displacement assays.^{18,19} Briefly, binding studies were carried out using 50 μL of 3 nM

[^3H]CP-55940 with 100 μL of 5 μg human CB_2 membrane protein (PerkinElmer Life Sciences), 30 μL of binding buffer (50 mM Tris-HCl, 2.5 mM EGTA, 5 mM MgCl_2 , and 0.5 mg/mL fatty acid free-bovine serum albumin), and 20 μL of substrate at various concentrations. After 1 h of incubation at 30°C , the mixture was filtered through UniFilter GF/B (PerkinElmer) and washed three to four times with ice cold washing buffer (50 mM Tris-HCl, 2.5 mM EGTA, 5 mM MgCl_2 , 2% bovine serum albumin, pH 7.4). After the plates were dried overnight, 30 μL of MicroScint O (PerkinElmer) was added to each well. The filter plate was kept in dark for 15 min before being counted using a TopCount scintillation counter (PerkinElmer). Inhibition constants (K_i) were calculated using GraphPad Prism 7.

2.5 Development of CPM Assay

A mixture of tested compound (5 μM of IR700DX-TK-*mbc94* or IR700DX-*mbc94*, or 1 μM of disulfide **4** or thiol **5**) and 100 μM of CPM in PBS buffer were added to 96-well plate. The light irradiated groups were irradiated with LED light (L690-66-60, Marubeni America Co., New York, New York) at wavelengths of 670 to 710 nm (peak at 690 nm) and a power density of 30 mW/cm^2 for 30 min (54 J/cm^2). The control groups were kept under ambient light for 30 min. The results were obtained using fluorescence plate reader with an excitation wavelength of 384 nm and emission wavelength of 470 nm to quantify the amount of activated CPM.

2.6 Time-Dependent CPM Assay Study

A mixture of tested compounds (5 μM of IR700DX-TK-*mbc94*, IR700DX-*mbc94* or IR700DX) and 100 μM of CPM in PBS buffer was added to 96-well plate. The light irradiated groups

were irradiated with LED light at wavelengths of 670 to 710 nm and a power density of 30 mW/cm² as measured with an optical power meter (PM100, Thorlabs) for 5-min interval up to 30 min total irradiation time. The results were obtained using fluorescence plate reader with an excitation wavelength of 384 nm and emission wavelength of 470 nm to quantify the amount of activated CPM.

2.7 ROS Production

To determine the types of ROS produced by IR700DX-TK-mbc94 and IR700DX-mbc94, 5 μM of IR700DX-TK-mbc94 or IR700DX-mbc94 was irradiated with LED light at wavelengths of 670 to 710 nm and a power density of 30 mW/cm² 5-min interval up to 30-min total irradiation time. ROS production was determined using 10 μM of the free-radical indicator, aminophenyl fluorescein (APF, Molecular Probes), or 10 μM of the singlet oxygen (¹O₂) sensor green (SOSG, Molecular Probes). Fluorescence intensities of APF at 500 nm (excitation at 480 nm) or that of SOSG at 520 nm (excitation at 500 nm) were recorded using a Synergy™ H4 hybrid multimode microplate reader.

2.8 Cell Culture

CB₂-mid DBT is a transfected mouse delayed brain tumor cell line expressing CB₂R at the endogenous levels.²⁰ CB₂-mid DBT cells were cultured in DMEM containing 10% fetal bovine serum, 4 mM glutamine, 100 units/mL penicillin, and 100 μg/mL streptomycin, the same methods as described in our previously published work.²¹

2.9 In Vitro PDT Study

CB₂-mid DBT cells were grown to confluence in T75 flasks, harvested, seeded into 96-well optical plates, and incubated in a water-jacketed incubator for 24 h prior to treatment. Cells were incubated with 0.5 or 1 μM of IR700DX-TK-mbc94 or IR700DX-mbc94 at 37°C overnight and cell medium was then replaced with fresh medium to remove unbound PS. Next, cells were irradiated with an LED light with wavelengths of 670 to 710 nm and a power density of 30 mW/cm² for 30 min, as measured with an optical power meter (PM100, Thorlabs). Cell viability was determined by CellTiter-Glo Luminescent Cell Viability Assay kit (Promega) right after or 24-h post-PDT treatment. For light dose-dependent PDT study, cells were treated with 1 or 2 μM of IR700DX-TK-mbc94 and three light doses were used, including 18 J/cm² (10 min of 30 mW/cm² irradiation), 36 J/cm² (20 min), and 54 J/cm² (30 min). Cell viability was measured right after PDT treatment.

2.10 Blocking Study

For the blocking group, cells in serum free medium was pretreated with 10 μM of the blocking agent SR144528 for 30 min, before being treated with 1 μM of IR700DX-TK-mbc94 for additional 30 min. Cells were then washed twice with serum free medium and fluorescence intensities at Ex/Em 620/690 nm were recorded using a Synergy™ H4 hybrid multimode microplate reader.

2.11 Data Processing

All data given in this study are the mean ± standard error of the mean (SEM) of *n* independent measurements (*n* = 4 for *in vitro* study). Statistical analyses were performed using the student *t*-test method, with *p* values < 0.05 considered statistically significant. Graphs were processed using GraphPad Prism 7 (GraphPad Software, Inc., La Jolla, California).

3 Results

Previously, we described the synthesis of compound **1**,⁸ a heterobifunctional ROS-responsive thioketal linker, where the two distinct functional groups provide readily assessable point for conventional amide coupling. This unique feature renders compound **1** an excellent ROS-activatable linker connecting two functionalities, a phthalocyanine PS, IR700DX and a cannabinoid, mbc94 (Fig. 2). Intermediate **2a** was prepared by coupling mbc94 and **1** via amide coupling using HBTU. The trifluoroacetamide protection was then removed using base hydrolysis to give **2b**. Finally, **2b** was mixed with IR700DX-NHS in dimethyl sulfoxide to yield compound IR700DX-TK-mbc94 (**3**). To study the therapeutic effect of the activated prodrug, we also synthesized mbc94-SH by attaching 3-(tritylthio) propionic acid to mbc94 through amide coupling, followed by deprotection of the thiol group in an acidic condition (Fig. 3). We found that IR700DX-TK-mbc94 and IR700DX-mbc94 efficiently displaced the high-affinity radioligand [³H]CP-55940 (*K_d* = 0.39 nM) from human CB₂R protein with similar nanomolar affinities (*K_i* = 2.67 ± 1.78 nM for IR700DX-TK-mbc94 versus 1.86 ± 1.38 nM for IR700DX-mbc94), which are roughly 20-fold higher than mbc94-SH (*K_i* = 47.7 ± 16 nM).

To validate the hypothesis that the thioketal linker is cleavable by the *in situ* generation of ROS, we quantified the amount of thiol generation upon light irradiation. We originally attempted to use the classic Ellman's assay for thiol quantitation.^{22,23} Unfortunately, this method is not suitable as the Ellman's reagent is prone to artifacts from redox reaction, which is inevitable due to the ROS generation. We therefore used the 7-diethylamino-3-(4'-maleimidylphenyl)-4-methylcoumarin (CPM) assay^{24,25} to determine the ROS-induced thioketal cleavage. CPM is a weakly fluorescent compound but its fluorescent can be activated upon reaction with thiol via maleimide-thiol coupling reaction.^{26,27}

Upon light irradiation, IR700DX generates ROS, which can cleave the nearby thioketal linker and subsequently produce two thiol fragments and one acetone. As expected, over the 30-min light irradiation period, we observed steady increase of fluorescence from CPM mixed with IR700DX-TK-mbc94 (Fig. 4). Light irradiation of IR700DX-mbc94 and IR700DX caused similarly low level of CPM fluorescence and the vehicle group showed negligible signal, suggesting that ROS production alone may also lead to CPM fluorescence activation. Nevertheless, CPM fluorescence caused by light activation of IR700DX-TK-mbc94 is much higher than the other groups (*p* < 0.0001). To investigate whether the increased CPM fluorescence may be caused by higher level of ROS production, we further compared type I and type II ROS produced from IR700DX-TK-mbc94 and IR700DX-mbc94 (Fig. 5). Under the same dose of light irradiation, IR700DX-TK-mbc94 produced almost the same amount of type I (APF indicating free radical, RFU APF: 7731 for IR700DX-TK-mbc94 versus 7760 for IR700DX-mbc94 after 30-min irradiation), and less amount of type II (SOSG indicating singlet oxygen, RFU SOSG: 8901 for IR700DX-TK-mbc94

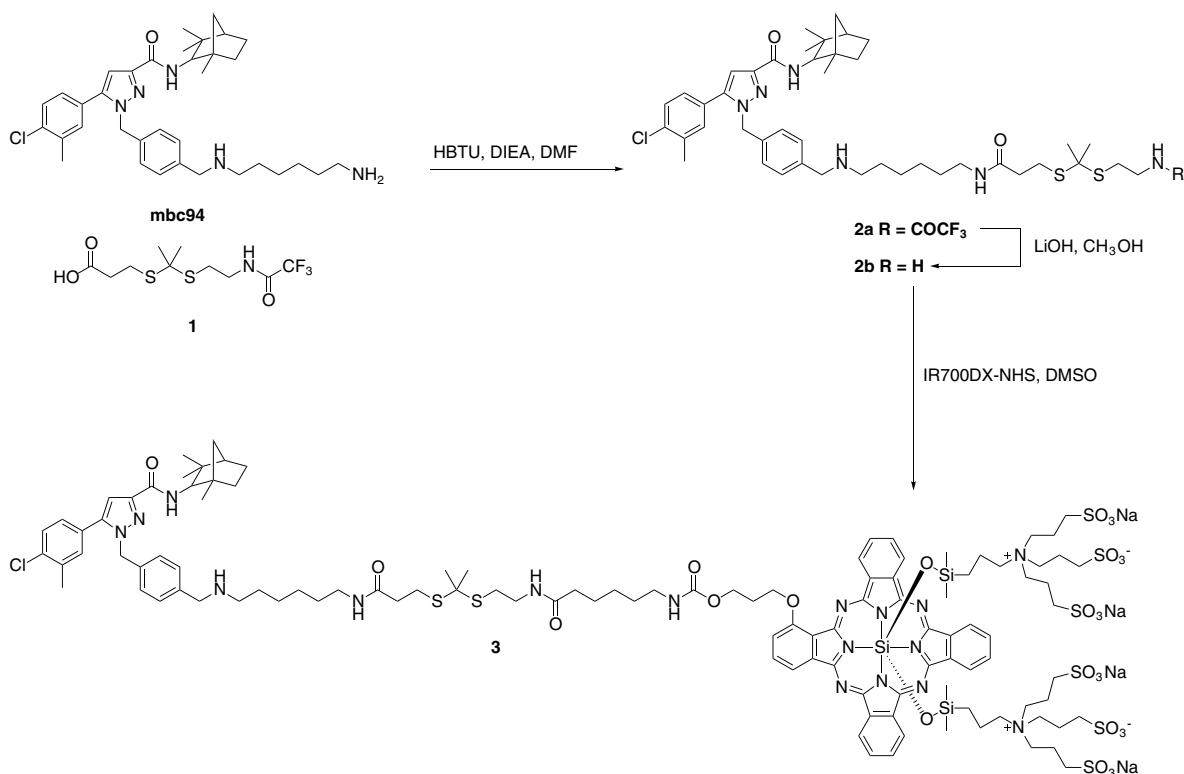


Fig. 2 Synthesis of IR700DX-TK-mbc94.

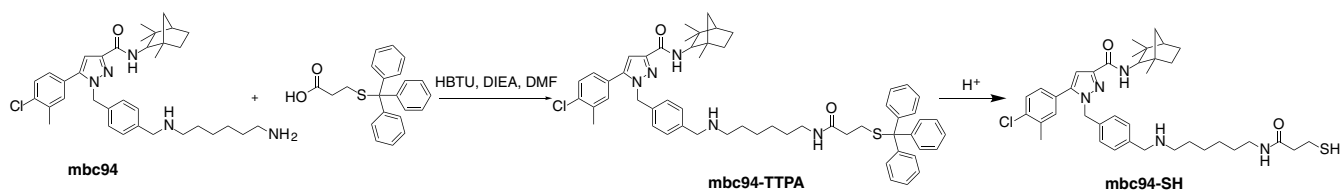


Fig. 3 Synthesis of mbc94-SH.

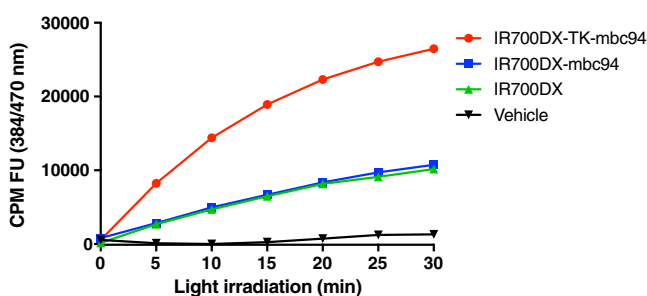


Fig. 4 Fluorescence intensity of CPM over 30 min of light irradiation at 690 nm is compared among four groups, including IR700DX-TK-mbc94, IR700DX-mbc94, IR700DX, and vehicle.

versus 11412 for IR700DX-mbc94 after 30-min irradiation, 22% less) ROS than IR700DX-mbc94, indicating that ROS production did not contribute to the increased CPM fluorescence in the IR700DX-TK-mbc94 group. These combined data suggest that thiol production from IR700DX-TK-mbc94 dominated the CPM fluorescence activation.

The *in vitro* therapeutic results are summarized in Fig. 6. To demonstrate the advantages of the light-activatable combination

therapy strategy, all therapeutic results are compared between IR700DX-TK-mbc94 and the nonactivatable IR700DX-mbc94 analog. Experimental setup is demonstrated in Fig. 7. To ensure uniform light irradiation, light dose was determined using an optical power meter and each group of cells ($n = 4$) was positioned in the center of the irradiated region. We first treated CB₂R+ mouse delayed brain tumor CB₂-mid DBT cells with two concentrations (0.5 and 1 μM) of IR700DX-TK-mbc94 or IR700DX-mbc94, washed unbound PSs, and applied light irradiation [Figs. 6(a) and 6(b)]. We found that right after light irradiation, 59% death was observed in cells treated with 1 μM of IR700DX-TK-mbc94, whereas no significant cell death was seen in the IR700DX-mbc94 treatment group ($p < 0.0001$). After these cells were incubated for additional 24 h, the IR700DX-TK-mbc94 treatment group showed increased cell death to 97% and the IR700DX-mbc94 group showed 74% cell death ($p = 0.001$), suggesting that programmatic apoptotic cell death was involved in both groups, but necrosis was only involved in the IR700DX-TK-mbc94 group. At the lower PS concentration (0.5 μM), no significant cell death was observed in either group right after light irradiation; however, after additional 24 h incubation, the IR700DX-TK-mbc94 group showed 78% cell death as compared to insignificant cell death in the

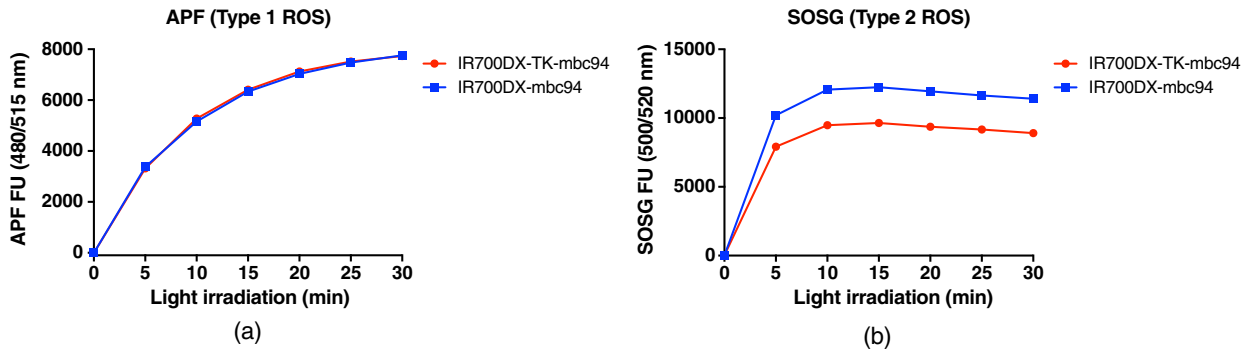


Fig. 5 ROS production of IR700DX-TK-mbc94 and IR700DX-mbc94 analyzed by (a) APF (type I ROS) and (b) SOSG (type II ROS) assays.

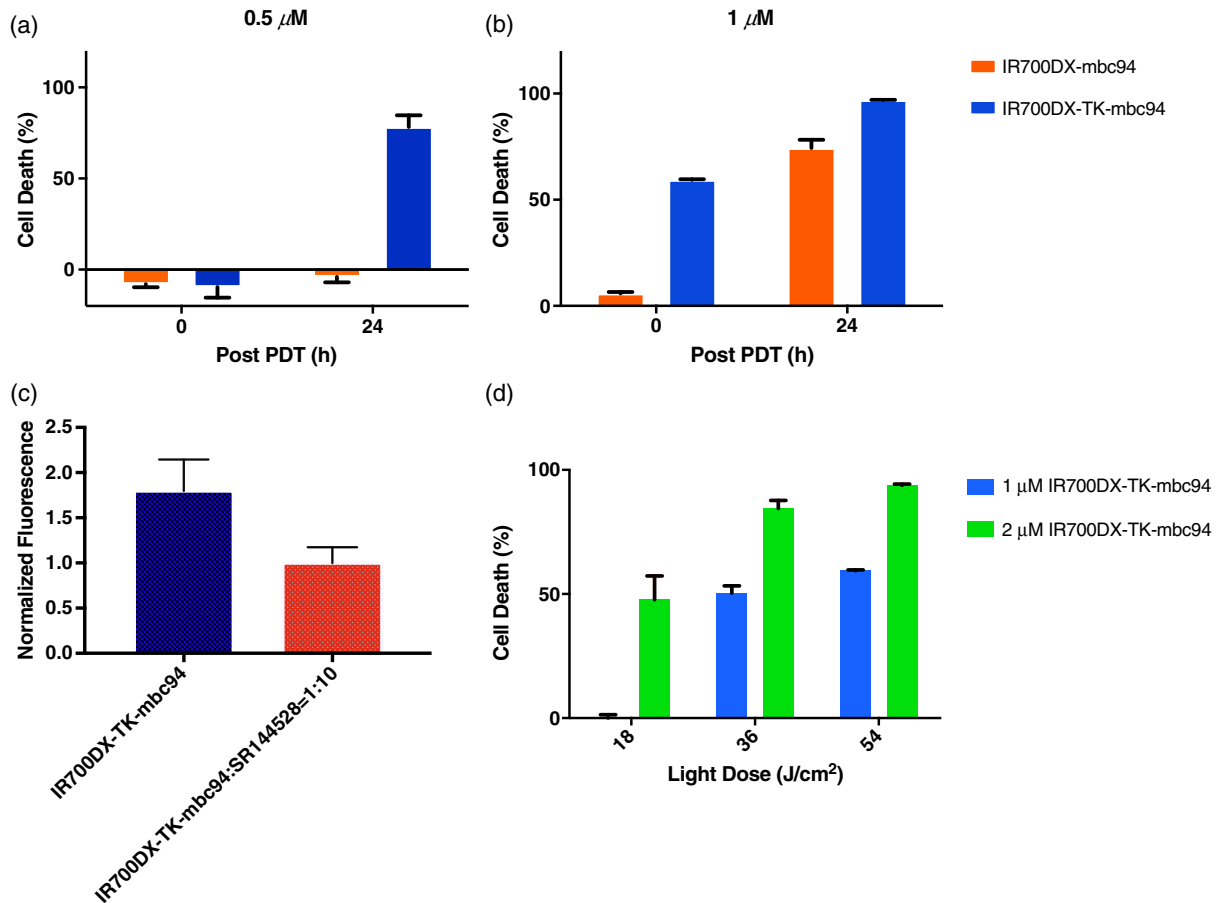


Fig. 6 PDT treatment using IR700DX-TK-mbc94 led to increased cancer cell death as compared to PDT with IR700DX-mbc94. (a,b) Concentration-dependent and progressive cell death caused by PDT using (a) 0.5 or (b) 1 μM IR700DX-TK-mbc94 or IR700DX-mbc94. Progressive cell death was observed after PDT treatment (24 h post-PDT versus right after PDT treatment). (c) Cellular uptake of IR700DX-TK-mbc94 can be blocked by a CB₂R ligand, SR144528. (d) Light dose-dependent cell death caused by PDT using IR700DX-TK-mbc94. Cells were treated with 18, 36, or 54 J/cm² 690-nm light after incubation with 1 or 2 μM IR700DX-TK-mbc94.

IR700DX-mbc94 group ($p < 0.0001$). In addition, we found that the cellular uptake of IR700DX-TK-mbc94 group can be significantly blocked by the CB₂R ligand SR144528 [44% blocking effect, $p = 0.02$, Fig. 6(c)], supporting target-specific binding of IR700DX-TK-mbc94. We also studied light dose-dependent therapy using three light doses (18, 36, and 54 J/cm²)

and two concentrations (1 and 2 μM) [Fig. 6(d)]. It is obvious that higher light dose or concentration led to greater cell death. Interestingly, mbc94-SH alone did not cause significant cell death (Fig. 8). We also found that although light treatment using IR700DX-TK-mbc94 caused almost complete death of CB₂-mid DBT cells, the same treatment appears to be safe to

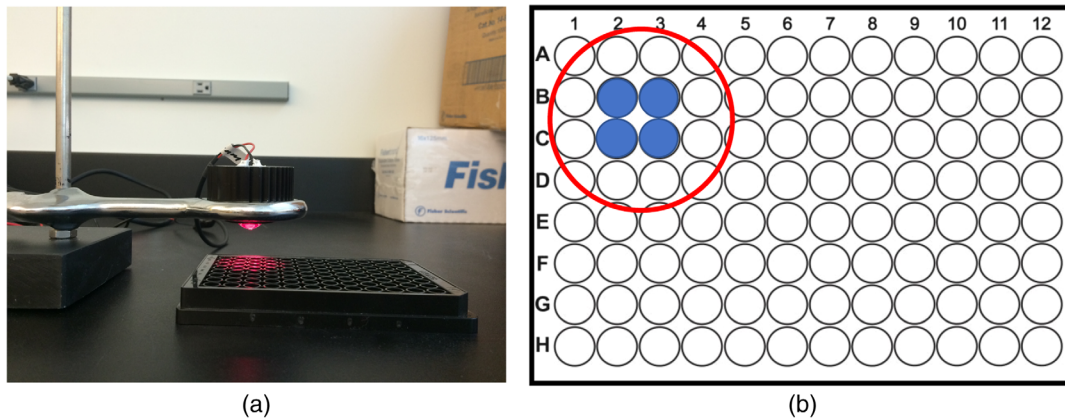


Fig. 7 *In vitro* PDT study using 96-well plates. (a) LED light was used to irradiate cells treated with IR700DX-TK-*mbc94* or IR700DX-*mbc94*. (b) To ensure uniform light irradiation, light dose was determined using an optical power meter and each group of cells ($n = 4$) was positioned in the center of the irradiated region. Other groups of cells were positioned outside of the irradiated region.

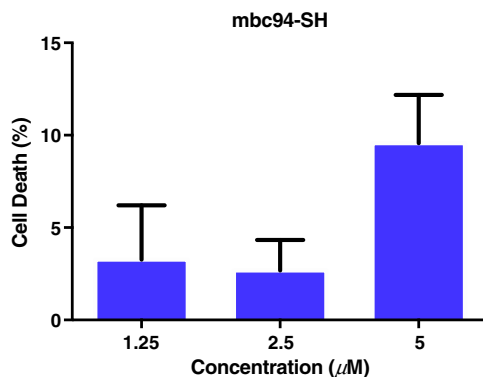


Fig. 8 *mbc94*-SH alone is not efficient in cancer cell treatment.

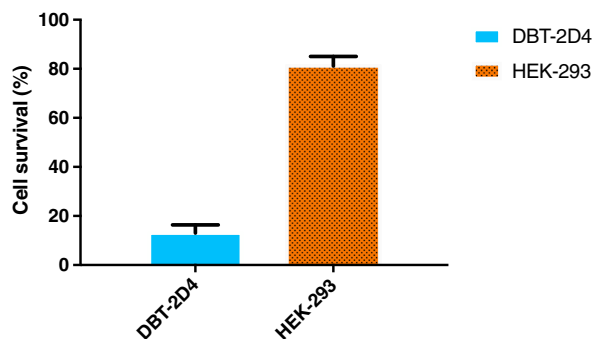


Fig. 9 Normal cell control (HEK-293) showed negligible death as compared to CB_2R -expressing DBT-2D4 cells after treatment with PDT using $2 \mu\text{M}$ IR700DX-TK-*mbc94* and $54 \text{ J}/\text{cm}^2$ light dose.

HEK-293 normal cell control (Fig. 9). These data suggest that IR700DX-TK-*mbc94* is remarkably effective in treating cancer cells in a target-specific manner.

4 Discussion

The combination of multiple therapeutics for cancer treatment has gained growing interest. Such a practice usually leads to enhanced outcome. In some cases, more favorable synergistic effects are achieved, offering remarkable therapeutic outcome

and fewer side effects. Recently, we demonstrated the synergistic outcome by combining two PDT agents that bind to distinct cellular localization.⁶ Although combination therapy can be easily realized by administration of multiple therapeutics individually, a more attractive approach is targeted delivery of therapeutics to the tumor site in one package, where they can be activated or released on demand. This approach is likely to further improve the therapeutic outcome and safety. Often, a cleavable linker is included in the drug delivery system design that is sensitive to conditions associated with tumor cells or micro-environment, such as protease, acidic pH, and oxidative stress.²⁸ Although dozens of cleavable linkers have been developed, the cleavage is usually controlled only spatially, but not temporally. In addition, these drug delivery systems are typically difficult to develop, involving multifunctional nanosystems or small molecules with many components. Here, we aimed to develop a multifunctional prodrug, which has a simple design but allows for targeted combinatory therapy and on-demand activation both spatially and temporally. This was achieved by utilizing a unique ROS-activatable heterobifunctional linker, a CB_2R -targeted cannabinoid prodrug, and a highly hydrophilic PS with six sulfonate groups.

One interesting finding is that both IR700DX-TK-*mbc94* and IR700DX-*mbc94* bind to CB_2R with a much higher (~ 20 folds) affinity than *mbc94*-SH. This is surprising because typically attachment of a large dye molecule to a small targeting ligand compromises the binding, as we have observed in our previous studies.^{19,29} Although the exact binding mechanism is yet to be investigated, it is possible that IR700DX facilitated the interaction by binding to additional sites on CB_2R . It has been previously reported that phthalocyanine dyes can bind to certain proteins.³⁰ It is noteworthy that the binding affinity of IR700DX-*mbc94* to CB_2R has been previously reported by us determined by live cell fluorescence binding study ($K_d = 42 \text{ nM}$), which is considerably lower than the binding affinity reported in this study ($K_i = 1.86 \text{ nM}$). However, such a significant difference is not surprising, because the previous binding study used live murine cells but human CB_2R protein was used in this binding study. Our previous study has shown that largely different binding affinities were determined when protein versus intact cells were used.³¹ In addition, human and mouse CB_2Rs only share 82% amino acid identity.³²

IR700DX-TK-mbc94 and IR700DX-mbc94 share the same PS and therefore, the amount of ROS produced from each agent is presumed to be the same. However, based on the SOSG studies, the singlet oxygen produced from IR700DX-TK-mbc94 appears to be less than that from IR700DX-mbc94. This is in fact expected because some singlet oxygen produced from IR700DX-TK-mbc94 was consumed to cleave the ROS-activatable thioketal linker and therefore not able to be detected by SOSG. Because singlet oxygen is the main phototoxicity source from IR700DX,⁴ such loss of singlet oxygen would reduce the therapeutic outcome of IR700DX-TK-mbc94 as compared to IR700DX-mbc94. In contrast, we found that IR700DX-TK-mbc94 produced much higher therapeutic outcome than IR700DX-mbc94, suggesting that the ROS-activated prodrug, mbc94-SH, greatly contributed to the treatment. Interestingly, mbc94-SH alone, even with a concentration of 5 μ M, did not show significant therapeutic effect, whereas IR700DX-TK-mbc94 treatment with much lower concentrations caused dramatic cell death. We speculate that IR700DX-TK-mbc94, which has a higher binding affinity to CB₂R than mbc94-SH, facilitated delivery of mbc94-SH to the target site. As a result, mbc94-SH cleaved from IR700DX-TK-mbc94 is more effective than if it is directly used to treat CB₂R+ cells. It is also possible that the remarkable therapeutic outcome from IR700DX-TK-mbc94 is attributed to the synergism between PDT and cannabinoid therapy.

5 Conclusions

In conclusion, we developed a far red light-activatable prodrug, IR700DX-TK-mbc94, which binds to CB₂R with a nanomolar affinity and synergizes PDT and cannabinoid therapy. IR700DX-TK-mbc94 showed superior efficacy than IR700DX-mbc94 in the therapeutic studies. With many favorable features including targeting specificity, on-demand activation, combinatory therapy, high hydrophilicity and safety, IR700DX-TK-mbc94 has great potential in treating CB₂R-positive tumors.

Disclosures

The authors have submitted a provisional patent based on the IR700DX-TK-mbc94 design and have no potential conflicts of interest to disclose.

Acknowledgments

We thank Dr. Nephi Stella from the University of Washington for providing CB₂-mid DBT cells and Dr. Fan Zhong from Fudan University for providing advice on statistical analysis.

References

1. D. E. Dolmans, D. Fukumura, and R. K. Jain, "Photodynamic therapy for cancer," *Nat. Rev. Cancer* **3**(5), 380–387 (2003).
2. Z. Huang, "A review of progress in clinical photodynamic therapy," *Technol. Cancer Res. Treat.* **4**(3), 283–293 (2005).
3. M. Triesscheijn et al., "Photodynamic therapy in oncology," *Oncologist* **11**(9), 1034–1044 (2006).
4. N. Y. Jia et al., "Cannabinoid CB₂ receptor as a new phototherapy target for the inhibition of tumor growth," *Mol. Pharmacol.* **11**(6), 1919–1929 (2014).
5. S. Zhang et al., "Target-selective phototherapy using a ligand-based photosensitizer for type 2 cannabinoid receptor," *Chem. Biol.* **21**(3), 338–344 (2014).
6. L. Yang et al., "Multilayer photodynamic therapy for highly effective and safe cancer treatment," *Acta Biomater.* **54**, 271–280 (2017).

7. S. Zhang et al., "Tumor mitochondria-targeted photodynamic therapy with a translocator protein (TSPO)-specific photosensitizer," *Acta Biomater.* **28**, 160–170 (2015).
8. X. Ling et al., "Synthesis of a reactive oxygen species responsive heterobifunctional thioketal linker," *Tetrahedron. Lett.* **56**(37), 5242–5244 (2015).
9. M. Bio et al., "Site-specific and far-red-light-activatable prodrug of combretastatin A-4 using photo-unclick chemistry," *J. Med. Chem.* **56**(10), 3936–3942 (2013).
10. M. Bio et al., "Far-red light activatable, multifunctional prodrug for fluorescence optical imaging and combinational treatment," *J. Med. Chem.* **57**(8), 3401–3409 (2014).
11. G. Nkepan et al., "Folate receptor-mediated enhanced and specific delivery of far-red light-activatable prodrugs of combretastatin A-4 to FR-positive tumor," *Bioconjugate Chem.* **25**(12), 2175–2188 (2014).
12. M. Bio et al., "Efficient activation of a visible light-activatable CA4 prodrug through intermolecular photo-unclick chemistry in mitochondria," *Chem. Commun.* **53**(11), 1884–1887 (2017).
13. P. Thapa et al., "Far-red light-activatable prodrug of paclitaxel for the combined effects of photodynamic therapy and site-specific paclitaxel chemotherapy," *J. Med. Chem.* **59**(7), 3204–3214 (2016).
14. P. Thapa et al., "Folate-PEG conjugates of a far-red light-activatable paclitaxel prodrug to improve selectivity toward folate receptor-positive cancer cells," *ACS Omega* **2**(10), 6349–6360 (2017).
15. S. D. McAllister, L. Soroceanu, and P. Y. Desprez, "The antitumor activity of plant-derived non-psychoactive cannabinoids," *J. Neuroimmune Pharmacol.* **10**(2), 255–267 (2015).
16. F. A. Javid et al., "Cannabinoid pharmacology in cancer research: a new hope for cancer patients?" *Eur. J. Pharmacol.* **775**, 1–14 (2016).
17. B. Chakravarti, J. Ravi, and R. K. Ganju, "Cannabinoids as therapeutic agents in cancer: current status and future implications," *Oncotarget* **5**(15), 5852–5872 (2014).
18. S. Raduner et al., "Alkylamides from Echinacea are a new class of cannabinomimetics. Cannabinoid type 2 receptor-dependent and -independent immunomodulatory effects," *J. Biol. Chem.* **281**(20), 14192–14206 (2006).
19. M. Sexton et al., "NIR-mbc94, a fluorescent ligand that binds to endogenous CB₂ receptors and is amenable to high-throughput screening," *Chem. Biol.* **18**(5), 563–568 (2011).
20. E. Cudaback et al., "The expression level of CB₁ and CB₂ receptors determines their efficacy at inducing apoptosis in astrocytomas," *PLoS One* **5**(1), e8702 (2011).
21. S. Zhang, P. Shao, and M. Bai, "In vivo type 2 cannabinoid receptor-targeted tumor optical imaging using a near infrared fluorescent probe," *Bioconjugate Chem.* **24**(11), 1907–1916 (2013).
22. G. L. Ellman, "Tissue sulfhydryl groups," *Arch. Biochem. Biophys.* **82**(1), 70–77 (1959).
23. P. W. Riddles, R. L. Blakeley, and B. Zerner, "Reassessment of Ellman's reagent," *Methods Enzymol.* **91**, 49–60 (1983).
24. C. C. Chung et al., "A fluorescence-based thiol quantification assay for ultra-high-throughput screening for inhibitors of coenzyme a production," *Assay Drug Dev. Technol.* **6**(3), 361–374 (2008).
25. T. O. Sippel, "New fluorochromes for thiols: maleimide and iodoacetamide derivatives of a 3-phenylcoumarin fluorophore," *J. Histochem. Cytochem.* **29**(2), 314–316 (1981).
26. D. P. Nair et al., "The thiol-Michael addition click reaction: a powerful and widely used tool in materials chemistry," *Chem. Mater.* **26**(1), 724–744 (2014).
27. S. S. Ghosh et al., "Use of maleimide-thiol coupling chemistry for efficient syntheses of oligonucleotide-enzyme conjugate hybridization probes," *Bioconjugate Chem.* **1**(1), 71–76 (2002).
28. G. Leriche, L. Chisholm, and A. Wagner, "Cleavable linkers in chemical biology," *Bio-organ. Med. Chem.* **20**(2), 571–582 (2012).
29. M. F. Bai et al., "MBC94, a conjugable ligand for cannabinoid CB₂ receptor imaging," *Bioconjugate Chem.* **19**(5), 988–992 (2008).
30. R. L. Morris et al., "The peripheral benzodiazepine receptor in photodynamic therapy with the phthalocyanine photosensitizer Pc 4," *Photochem. Photobiol.* **75**(6), 652–661 (2002).
31. M. Sexton et al., "Binding of NIR-conPK and NIR-6T to astrocytomas and microglial cells: evidence for a protein related to TSPO," *PLoS One* **4**(12), e8271 (2009).

32. D. Shire et al., "Molecular cloning, expression and function of the murine CB2 peripheral cannabinoid receptor," *Biochim. Biophys. Acta* **1307**(2), 132–136 (1996).

Mingfeng Bai received his BS degree in chemistry from Nankai University and his MS and PhD degrees in chemistry from Vanderbilt University. He is an assistant professor of radiology and

radiological sciences at VUMC. The goal of his laboratory is to develop and evaluate new molecular probes for intraoperative imaging and therapy, particularly fluorescence imaging agents and photosensitizers with the ultimate goal of moving the basic science discoveries to the clinic.

Biographies for the other authors are not available.